An Altitude Control Strategy for Biomass

Javier Sánchez[(1)], Pere Ramos Bosch[(1)], Daniel Ranuschio[(2)], and Helena Mainka[(3)]

[(1)] European Space Agency (ESOC)
Darmstadt, Germany
Email: javier.sanchez@esa.int
Email: pere.ramos.bosch@esa.int

[(2)] CS Group
Darmstadt, Germany
Email: daniel.ranuschio@ext.esa.int

[(3)] Telespazio Germany GmbH
Darmstadt, Germany
Email: helena.mainka@ext.esa.int

***Abstract* – The paper describes the altitude control strategy design for the Biomass mission before its launch. The spacecraft will be orbiting at an altitude of approximately 670 km in a sun-synchronous orbit. The operation of its instrument requires altitude variations with respect to its reference orbit to be strictly constrained, leading to the need of a precise eccentricity control. The mission is expected to undergo large perturbations on the eccentricity vector resulting from solar radiation pressure and air drag, owing to the spacecraft's large areas exposed to the Sun and its operational altitude. Additionally, the location of routine manoeuvres in the orbital arc is constrained to certain areas to avoid the interruption of scientific retrievals, which introduces additional eccentricity control constraints. The control strategy is developed by drawing an analogy with planar rigid body motion for the behaviour of the eccentricity vector under the effect of these perturbations.**

I. INTRODUCTION

Biomass is ESA's seventh Earth Explorer mission, dedicated to study the Earth's forests from space. It is equipped with a first of its kind, P-band Synthetic Aperture Radar (SAR), which will be used to retrieve information about the forest structure and derive parameters such as forest biomass and forest height. The Biomass mission will be operated from the European Space Operations Centre (ESOC) in Darmstadt, Germany.

The satellite will be operated at an altitude of approximately 670 km, in a sun-synchronous orbit, with a local time of the ascending node at 6 a.m. The mission anticipates a sophisticated observation scheme, defining two different segments: a tomographic (TOM), and an interferometric (INT) phase. In each one of these phases the spacecraft will be operated at a different altitude, introducing a westward drift with respect to a fixed ground track repeat pattern of 44 orbits in 3 days. The purpose of this drift in longitude is to take observations of the revisited areas with a specific baseline, which is different for each one of the mission segments.

The 44 orbits repeat pattern leads to a large inter-nodal distance of approximately 910 km. With a relatively narrow swath, and a slow westward drift, the mission profile defines two processes, which are part of the routine operations, to achieve global coverage. Firstly, the satellite is able to perform observations in three different roll attitudes; they are referred to as swath A, B, and C. Each one of the mission segments requires a specific number of scientific retrievals from the same geographical area: seven during the TOM phase, and three during the INT phase. Once a cycle of such observations has been finalised, the satellite can alternate to the next swath orientation, pointing the instrument farther to the west, and taking scientific retrievals of new areas. After finishing a loop of observations in the three attitudes A, B, and C, the satellite will perform an orbit relocation, by means of a Satellite Repositioning Manoeuvre (SRM), to a different orbital phase, which allows retrieving observations from areas farther to the west. A complete cycle, including observations in all three swaths plus a SRM is known as a major cycle. Major cycles are then repeated until global coverage is achieved. The time interval between one SRM and the next is different for each mission segment: in TOM phase, it is seven revisits for each one of the three swaths (A, B, C) times three days of the repeat cycle, which is equal to 63 days; for the INT phase, it is 27 days, since the number of required revisits is three.

Each SRM has a duration of nine days, over which a total longitude bias has to be achieved. The shift in longitude is the precise one to resume observations

over unmapped areas to the west, starting again with swath A. The drift start manoeuvre requires a Δv size which depends on the mission segment, but of the order of 1.4 m/s. After that follows a five-day drift period, which is concluded by a series of two drift stop manoeuvres to return to the original altitude.

During periods of scientific observation, the orbit maintenance is achieved by means of Orbit Control Maneouvres (OCM), keeping the operational orbit close to a reference ground track. This reference ground track is an optimized trajectory fulfilling the scientific requirements of the mission. In particular, it implements the westward drift necessary for each one of the mission segments. The objective of the orbit control is to keep the ground track deviation within a specific band with respect to the reference ground track. The size of the control band is ±578 m for the TOM phase, and ±497 m for the INT phase. The time period between OCMs has been chosen to be three days, the same value as the repeat cycle, in order to further improve the accuracy performances when overflying the same geographical areas.

Besides ground track control, the instrument requires the orbital altitude excursions to be within ±500 m with respect to the reference trajectory, which imposes a constraint on eccentricity control. At the same time, the perturbations on the eccentricity vector are expected to be relatively high, owing to the large size of the spacecraft, with an antenna 12 metres in diameter. Table 1 provides an approximation to the parameters defining the Solar Radiation Pressure (SRP) and atmospheric drag, which have been used to carry out the analysis presented in this paper.

Table 1: Assumed spacecraft characteristics.

Parameter:	Value:
Mass	1090 kg
SRP coefficient	1.3
SRP reference area	120 m^2
Drag coefficient	2.0
Drag reference area	20 m^2

The altitude control strategy for Biomass has been designed based on previous work done by the ESOC Flight Dynamics team, characterizing the eccentricity behaviour in the presence of perturbations such as the SRP [1] [2], and the atmospheric drag [3]. This approach allows understanding the eccentricity evolution drawing an analogy with planar rigid body motion, with an Instantaneous Centre of Rotation (ICR) progressing along the e_x, e_y plane. The main challenges to elaborate an eccentricity control strategy for Biomass are detailed hereinafter.

A. Solar Radiation Pressure

Biomass' large area exposed to the Sun direction leads to a high SRP force. Previous work showed that the ICR evolution due to the SRP follows an analemma-like trajectory (analemmoid), with a shape and extension function of the orbital plane orientation and the magnitude of the SRP force. The geometry of this analemmoid, compared to the eccentricity control threshold derived from the ±500 m constraint on altitude control, presents the first challenge to the eccentricity control.

B. Air drag

Analyses show that the ICR trajectory can also be influenced by the air drag perturbation [3]. This is, particularly, the case for missions operated at relatively low altitudes. The main reason of perturbation in the eccentricity vector is the asymmetry in the air drag force acting on the spacecraft along an orbit revolution. In the case of Biomass, it has been observed that the perturbation due to air drag may also have a noteworthy contribution in phases of high solar activity.

C. Longitude drift

Another potential eccentricity perturbation cause is the one associated to the special mission profile that was introduced above. Biomass will be operated following a reference trajectory drifting westwards with respect to a fixed ground track repeat pattern. That is, from one quasi repeat cycle to the next, the ground track is shifted to the west by a longitude difference, $\Delta\lambda$, equivalent to 5.887 km in the TOM phase, and 4.9725 km in the INT phase. This implies that the satellite will orbit over areas with different sectoral and tesseral Earth potential harmonics. The frozen eccentricity vector associated with the longitudes where the satellite is passing through will be evolving as the mission progresses, potentially changing the position of the ICR. This effect, however, can be neglected, as it will be shown in the next sections.

The subsequent sections are dedicated to describing in detail, firstly, the manoeuvre constraints applicable to the Biomass mission, and therefore, the impact they have in the controllability of the eccentricity vector; the analysis of the altitude control problem, deriving thresholds for the eccentricity control, and characterizing the behaviour of the ICR; and presenting the solution found for the Biomass mission. The analysis and results presented in this paper will show diagrams and make references to the e_x, e_y plane. It should be noted that the eccentricity vector represented in that plane is relative to that of the Biomass reference orbit at an equivalent argument of latitude position. Therefore, short-periodic variations are not visible.

II. BIOMASS MANOEUVRES

The mission foresees two types of manoeuvres. As defined in the introduction, SRMs are used to implement the orbital phase changes that are executed at the end of each major cycle. Their orbit location is unconstrained. Currently, the strategy foreseen for the SRMs execution is to perform one drift start manoeuvre, to raise the semi-major axis, followed by a drift stop split in two manoeuvres five and seven days later, respectively. Altitude constraints are not applicable during the drift phase, and the execution of these three large manoeuvres allows targeting any strategic position for the eccentricity vector before resuming scientific observations. The disadvantage of this manoeuvre type is the long time interval between them: 63 days during the TOM phase, and 27 during the INT. As it will be seen, there are time periods in the year where action on the eccentricity vector is required at a more frequent rate.

On the other hand, OCMs are executed during science observation periods. They must be executed in those areas where the instrument will not be in use in order not to interfere with the retrievals. Manoeuvre slots are derived from the areas where the satellite instrument shall not be used, these are: 1) large ocean and desert areas, which are not of scientific interest to the mission, 2) geographical areas in which the instrument cannot be used: US Space Object Tracking Radars (SOTR) exclusion zone [4]. After the analysis of these areas, an orbital arc has been identified, which represents the longest time interval without payload operations, and, therefore, the longest manoeuvre slot available without an impact in science. It has been depicted in Fig. 1 on the Earth's surface. The length in time is either 2.4 hours or 2.1 hours, the difference depending on the actual current longitude of Biomass along the mission profile. These are referred to as long and short slots, respectively.

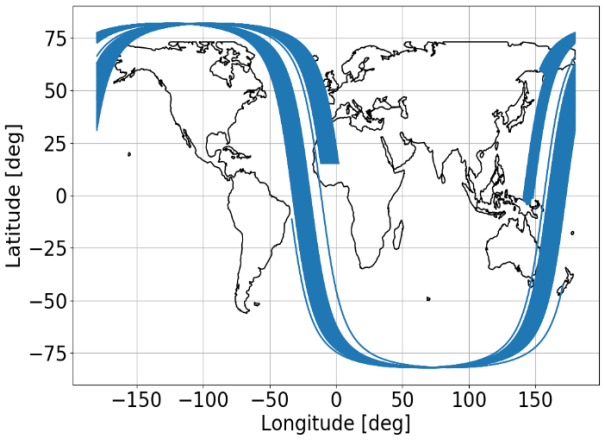

Fig. 1. Arc dedicated to orbit control maneouvres.

The spacecraft, however, requires a time of approximately 41 minutes from the last scientific observation to the start of the manoeuvre burn, and 39 minutes from the end of the manoeuvre burn to resume scientific observations. Taking this into account, the manoeuvre burn is, therefore, restricted to the orbital arc comprised between the arguments of latitude indicated in Table 2, which has been represented graphically in Fig. 2. Note that a manoeuvre executed in the velocity direction at a given argument of latitude will introduce a variation in the eccentricity vector, $\overrightarrow{\Delta e}$, in the direction given by that specific argument of latitude in the e_x, e_y plane. Therefore, the arcs depicted in Fig. 2 represent also the directions in which eccentricity variations are possible.

Table 2. Argument of latitude range for OCM execution.

Slot:	Start [deg]	End [deg]	Arc length[deg]
Long	165	40	235
Short	165	340	175

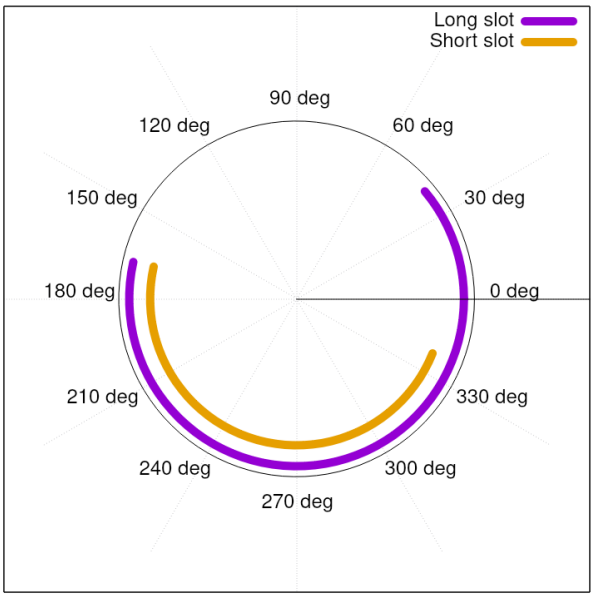

Fig. 2. Argument of latitude range for OCM execution.

III. ANALYSIS OF THE ALTITUDE CONTROL PROBLEM

The mission requires that altitude variations are within ±500 m with respect to a reference orbit. The first objective of this section is to translate this requirement into a variation of the orbital elements with respect to the reference orbit. For that, the following approximation is assumed: altitude deviations are approximated as radial deviations, linearized around a Keplerian orbit, as a function of the semi-major axis, a, the eccentricity, e, and the true anomaly, ν. Let (1) be the equation of an ellipse in polar form, centred at the

focus. The equation can be expressed as in (2), with the term ae^2 being of the order of 10 m for Biomass. The equation can be then re-written as in (3) and (4), with u and ω being the argument of latitude and the argument of perigee, and finally as in (5), with $\bar{e}$ and $\bar{u}$ being the eccentricity vector and a vector pointing at the orbit position given by the argument of latitude, respectively.

$$r = \frac{a(1-e^2)}{1+e\cos\nu} \quad (1)$$

$$r = a(1 - e\cos\,\nu\,) + O(ae^2) \quad (2)$$

$$r = a - ae\cos(u-\omega) \quad (3)$$

$$\mathrm{r} = a - ae\,(\cos u \quad \sin u)\begin{pmatrix}\cos\omega\\ \sin\omega\end{pmatrix} \quad (4)$$

$$\mathrm{r} = a - a\,\vec{u}\cdot\vec{e} \quad (5)$$

Differentiating (5), it is possible to obtain the expression shown in (6), with the four characteristic terms on its right-hand side that are described below in a qualitative manner.

$$\Delta r = \underbrace{\Delta a}_{1} - \underbrace{\Delta a(\vec{u}\cdot\vec{e})}_{2} - \underbrace{a(\overrightarrow{\Delta u}\cdot\vec{e})}_{3} - \underbrace{a(\vec{u}\cdot\overrightarrow{\Delta e})}_{4} \quad (6)$$

1. This term represents a change in altitude, due to a change in semi-major axis, homogeneously distributed along the orbit.
2. In an orbit with a given eccentricity, the altitude change introduced by a variation in semi-major axis is not homogeneously distributed along the orbit. This term is of the order of $e\Delta a$, and, therefore, negligible for an orbit like Biomass'.
3. For an orbit with a given eccentricity, this term represents the trivial change in radius vector as the satellite's argument of latitude evolves. Since altitude control requirements are expressed as maximum variations with respect to a reference orbit for the equivalent argument of latitude points, this term is not to be considered.
4. Change in altitude for a given variation in eccentricity vector.

The result of keeping the relevant terms for this problem is given in (7), and it shows that the altitude variations depend mainly on the variations in semi-major axis and eccentricity.

$$\Delta r \approx \Delta a - a(\vec{u}\cdot\overrightarrow{\Delta e}) \quad (7)$$

During routine operations, the variations in semi-major axis are determined by the energy losses due to air drag, which must be compensated for with OCMs; they are, therefore, a function of the solar activity. Numerical simulations, with historic values of the solar indices, were run with the objective of computing the Δv size required by the orbit control, assuming manoeuvre cycles of three days. The scenarios were selected to identify extreme cases, namely, with conditions close to a solar minimum (2009), solar maximum (2002), and a worst-case solar maximum (1991) with particularly high solar indices. With the value derived for the Δv and its associated semi-major axis variations, Δa, it is possible to compute via (6) the maximum eccentricity deviation value to comply with the ±500 m altitude requirement. The values for these thresholds are shown in Table 3, and they will be used throughout the analysis.

Table 3. Eccentricity threshold computed as a function of the orbit control Δv in different scenarios.

Δv [m/s]	e threshold	Notes
0.000	7.092E-5	No Δa control
0.002	7.066E-5	Solar minimum (2009)
0.060	6.294E-5	Solar maximum (2002)
0.080	6.028E-5	Solar maximum (1991)

The next step in the analysis is to compute the expected trajectory of the ICR. As advanced in the introduction, for Biomass there are three potential sources of eccentricity vector perturbation: SRP, air drag, and the change in longitude throughout the mission. The computation of the ICR for the cases considering the SRP and air drag as perturbing force has been done using equations (8), (9), and (10), extracted from [1], and derived from the Gauss form of the variational equations. In (8) and (9), we compute the eccentricity change rate due to the perturbation, $\dot{\vec{e}}_{pert}$, as a function of the perturbation in question, represented by $\vec{\gamma}$, the position, velocity, angular momentum of the orbit, and its derivative, respectively $\vec{r}$, $\vec{v}$, $\vec{h}$, and $\dot{\vec{h}}$. Finally, the eccentricity change rate due to the perturbation is superposed with the rotation around the frozen eccentricity induced by the Earth's potential. Using (10), it is possible to compute the position of the ICR as a function of the characteristic angular velocity of the eccentricity vector, $\vec{\Omega}$, and the previously derived value for $\dot{\vec{e}}_{pert}$. The value of $\vec{\Omega}$, can be derived either empirically, with the rotation period of the eccentricity around its frozen value free of perturbations other than the Earth's potential, or analytically with the expression given in [5]. Its value for the Biomass mission is -6.3897E-7 rad/s, which corresponds to a rotation period of approximately 113.81 days, rotating in the clock-wise direction.

$$\dot{\vec{e}}_{pert} = \frac{\vec{v}\times\dot{\vec{h}}}{\mu} + \frac{\vec{\gamma}\times\vec{h}}{\mu} \quad (8)$$

$$\dot{\vec{h}} = \vec{r}\times\vec{\gamma} \quad (9)$$

$$\overrightarrow{ICR} = \frac{\vec{\Omega}\times\dot{\vec{e}}}{\Omega^2} \quad (10)$$

The results for the ICR trajectory due to SRP and air drag are depicted in the e_x, e_y plane in Fig. 3 and Fig. 4, respectively. Both figures include the thresholds provided in Table 3, represented as circles around the centre of the figure, and labelled as *Thr 0*, *Thr 1*, *Thr 2*, and *Thr 3*, in an increasing order. As described in the introduction, the plot represents eccentricity deviations with respect to a reference orbit. Therefore, the point at the origin of the graph represents an orbit with an eccentricity equal to that of the reference orbit. The evolution of the ICR due to the SRP follows an analemmoid with a periodicity of one year due to the Sun's direction relative to the Biomass orbit. With a local time of the ascending node at 6 a.m., the analemmoid has approximately a symmetry axis along the e_y axis. Labels with the date (day and month) have been included to help mapping the position of the ICR along the year. The beta angle is smaller at the December solstice, leading to larger excursion during this part of the year than in the June solstice. The numerical computation of the ICR trajectory has been compared with an analytical computation, using the equations provided in [1], which is represented in lighter blue. The analytical computation does not consider the effect of the eclipses around the December solstice, and, therefore, provides an ICR position farther from the centre of the graph.

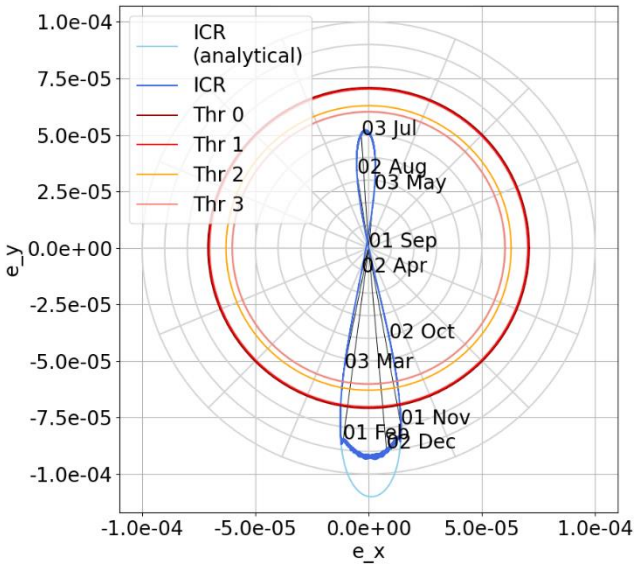

Fig. 3. Evolution of the ICR due to SRP.

The computation of the ICR due to the air drag perturbation has been done in an analogous manner, computing numerically the results of equations (8), (9), and (10), taking $\vec{\gamma}$ as the air drag force. The position of the ICR has been depicted in Fig. 4 in three different scenarios of low, medium, and high solar activity. From the results, it can be observed that the effect of the air drag can be neglected in any scenario other than the one corresponding to high solar activity. For those periods, the effect of the SRP and air drag can be considered additive; their combined effect has been depicted in Fig. 5.

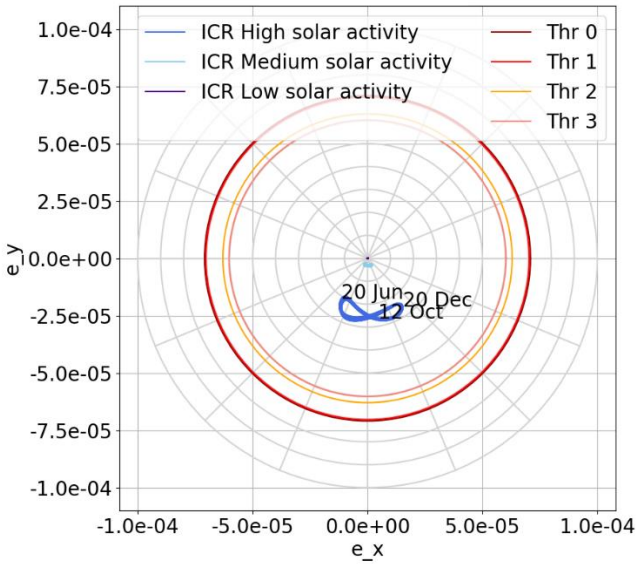

Fig. 4. Evolution of the ICR due to air drag.

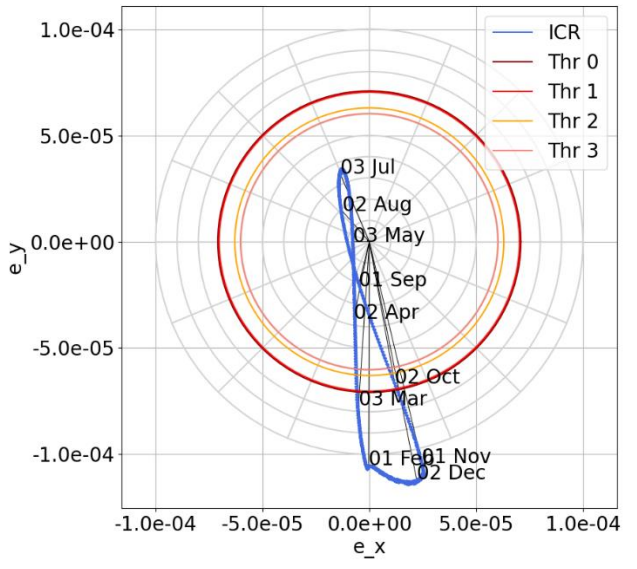

Fig. 5. Evolution of the ICR due to the combined effect of SRP and air drag in a scenario of high solar activity.

Finally, the last potential source of eccentricity perturbation has been analysed. Namely, the westward variation in longitude followed by the Biomass mission. To evaluate its effect, a set of orbits have been generated using only the Earth's potential, imposing the conditions of a 44-orbits repeat pattern in 3 days, local time at 6 a.m., frozen eccentricity, and each one of them with a different initial longitude taken from the interval from 0 to 8.2 degrees in steps of 0.1 degrees. The relative eccentricity of these orbits has been depicted in Fig. 6. The results show that the order of magnitude of these differences is much smaller than the scale represented in the previous plots. Therefore, this effect can be considered negligible for the eccentricity vector evolution.

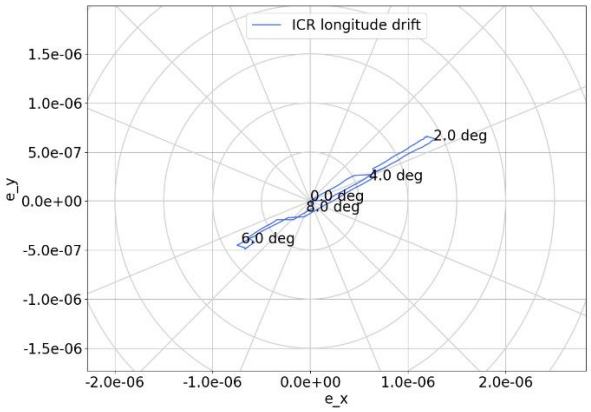

Fig. 6. Evolution of the ICR for different longitude values of the reference orbit.

IV. Identifying an Altitude Control Strategy

A numerical model has been developed, implementing the planar rigid body motion analogy equations [1] [2] for the eccentricity evolution. The Ordinary Differential Equation (ODE) represented in (11) provides the variation in eccentricity vector as a function of the eccentricity vector itself, the position of the ICR, which is a function of time, and $\vec{\Omega}$, which, at all effects, can be considered as a constant vector. The purpose of this model is to identify solution trajectories for the eccentricity vector, which can be used in the orbit control; they must be compliant with the eccentricity constraints, and, at the same time, be feasible to maintain with the restrictions in manoeuvre execution previously described. The ODE has been solved using a Runge-Kutta 45 method, giving initial conditions to the eccentricity vector.

$$\dot{\vec{e}} = \vec{\Omega} \times (\vec{e} - \overrightarrow{ICR}) \qquad (11)$$

The control strategy has been split in two different problems: A) Control close to the December solstice, where the ICR has a slow motion, and located outside of the control threshold for several months; and B) the eccentricity control for the rest of the year, following a path referred to as Lambda trajectory, similar to the solution found for the Sentinel-1 mission described in [2].

A. *The December solstice control*

From late October to late February, the ICR is located low in the e_x, e_y plane, and outside of the eccentricity control area delimited by the thresholds defined in Table 3. The strategy, in this case, consists of keeping the eccentricity vector following an arc close, but at an appropriate distance, of the ICR: it should be noted that leaving the eccentricity in free drift under these conditions, the longest permanence within the eccentricity thresholds is given by the arc between the tangents from the ICR to the eccentricity threshold. This is because, since the eccentricity rotates with constant angular velocity, the arc between the tangents provides the widest angular separation within the threshold. The trajectory in teal colour represented in Fig. 7 provides an example of such a solution, starting with initial condition at y_0*=(-5.0E-5, -5.0E-5)* on 1 December, and integrating up to 1 January. Considering the restrictions in manoeuvre direction depicted in Fig. 2, it is recommended to control the eccentricity on left half of the arc, so that the eccentricity changes implemented during routine orbit control can be tangent to the control arc. It can be verified that, in seasons of low solar activity, the available Δv for orbit maintenance every three days is enough to compensate for the rotation around the ICR.

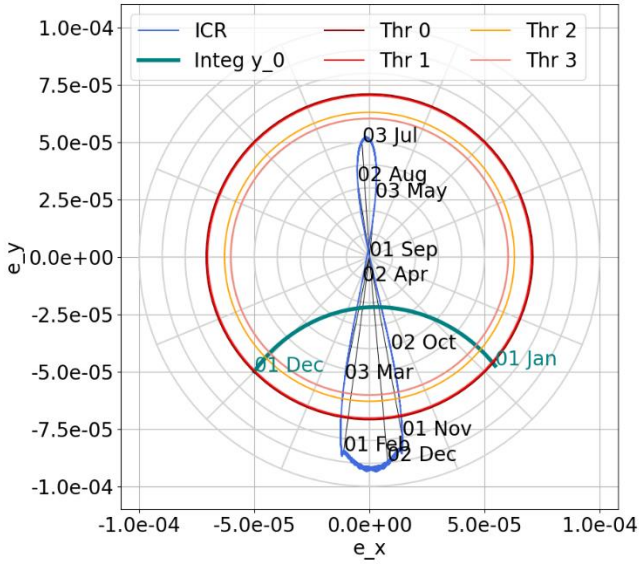

Fig. 7. Eccentricity control path during December solstice.

B. The Lambda trajectory

At the conclusion of the December solstice period the ICR ascends to the higher areas of the e_x, e_y plane, exhibiting a relatively rapid change in position compared to its motion during the December solstice. It should be noted that the eccentricity changes in the upward direction are significantly constrained, as it can be inferred from the constraints in manoeuvre location (see Fig. 2). The challenge at hand is to determine an appropriate initial condition for the eccentricity vector, allowing to follow the ICR's path towards its position at the June solstice.

The problem has been solved using the following method, depicted in Fig. 8. First, a trajectory has been integrated with initial condition at y_0*=(-5.0E-5,-5.0E-5)* on 1 February propagating its position five months into the future; it can be seen that this trajectory exceeds by far the eccentricity threshold in the upper part of the control area and it is, therefore, not suitable. The properties described in [2] applicable to this problem are that, under the perturbations that we have described, the eccentricity behaviour is analogous to planar rigid body motion. This means that, 1) there exists a moving rigid body (frame) in motion with respect to a fixed frame, the latter represented by the e_x, e_y axes, with the eccentricity motion represented by that of one point in the moving rigid body; as a corollary of the previous statement, the distances between points representing the evolution of eccentricity trajectories are preserved in the moving and in the fixed frame. Let us take two other initial conditions, y_1 and y_2, at the same epoch, forming a right triangle, and propagate their trajectories into the future. Three different snapshots of the right triangle have been taken, at the beginning, middle, and end of the propagation period, as shown in Fig. 8. It can be observed that the trajectory associated with the middle point of the small cathetus is suitable for the passage through the June solstice, between the ICR and the eccentricity threshold; the trajectory is also valid for the intermediate states, as it can be inferred from the evolutions from the first to the second and from the second to the third triangles.

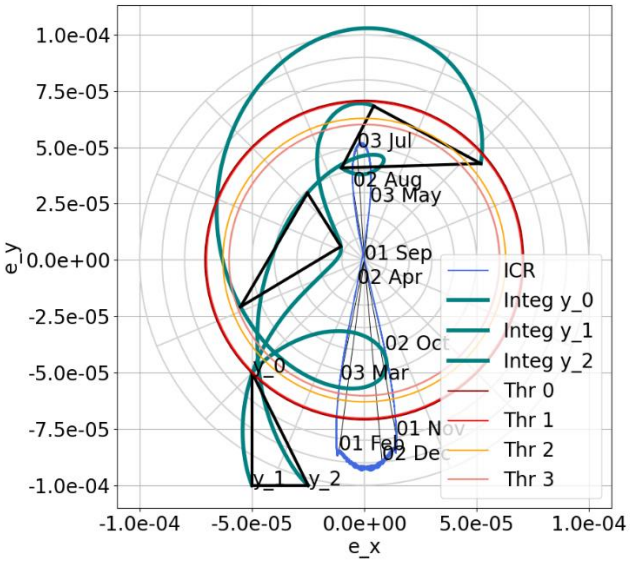

Fig. 8. Determination of a solution trajectory.

Finally, by selecting as initial condition the middle point of the small cathetus, y_λ*=(-3.75E-5, -1.0E-4)*, and integrating, it is possible to obtain the solution, which is referred to as the Lambda trajectory because of its characteristic shape. The integrated Lambda trajectory starts at y_λ on 1 February, which is outside of the eccentricity control area, and at the beginning of March the trajectory crosses the control threshold inwards. This is the point at which the control strategy has to transition from the December solstice control to acquire the Lambda trajectory.

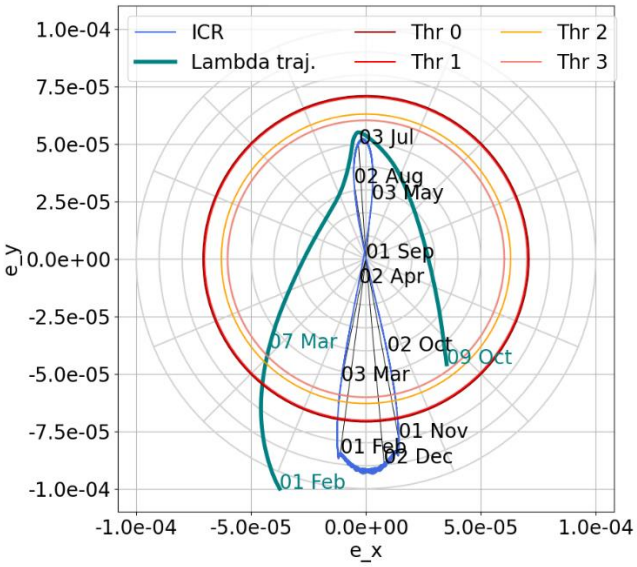

Fig. 9. Propagation of the initial conditions leading to the Lambda trajectory.

V. CONCLUSIONS

This paper outlines the methodology used to develop the altitude control strategy for the Biomass mission. Building upon previous research, the approach models the behaviour of the eccentricity vector in response to perturbations such as the SRP and air drag, and it makes use of the analogy established with planar rigid body motion.

By providing a comprehensive understanding of the eccentricity vector behaviour, this approach offers several advantages in identifying, in the first place, whether feasible solutions exist for the problem at hand. It also allows for the direct implementation of the solutions found in the orbit control, enhancing the effectiveness of the manoeuvre optimization process.

The strategy proposed for the Biomass mission implies controlling the eccentricity vector around an arc, separated a specific distance from the ICR, during the December solstice period. For the rest of the year, the strategy consists of acquiring the so-called Lambda trajectory, which is compliant with the constraints in eccentricity control.

In addition to the results outlined in this paper, there are several areas for future investigation that deserve attention. The proposed solution has to be integrated with the Biomass orbit control. This requires studying in detail several aspects, such as the transition from the December solstice control to the Lambda trajectory, and vice versa. Finally, the model needs to be calibrated during actual operations, as it is based on parameters for which the knowledge of their values is rather poor before launch. This is the case of the parameters defining the SRP force and the air drag.

VI. REFERENCES

[1] Sánchez, J., Martín Serrano, M.A., and Mackenzie, R., *"Characterization of the Solar Radiation Pressure Perturbation in the Eccentricity Vector"*. Proceedings 25th International Symposium on Space Flight Dynamics - 25th ISSFD. Munich, Germany, 2015.

[2] Sánchez, J., Kuchynka, P., *"Analysis of the Eccentricity Vector in Low Earth Orbits as Planar Rigid Body Motion"*. Proceedings 26th International Symposium on Space Flight Dynamics - 26th ISSFD. Matsuyama, Japan, 2016.

[3] Sánchez, J., Vasconcelos, A., *"Effect of the Air Drag Perturbation in the Eccentricity Vector for Very Low Earth Orbits"*. Proceedings 27th International Symposium on Space Flight Dynamics - 27th ISSFD. Melbourne, Australia, 2019.

[4] Heliere, F., Fois, F., Lin, Chung-Chi, Scipal, K., Arcioni, M., Bensi, P., Davidson, M., Silvestrin, P., Drinkwater, M., Meynart, R., *"Biomass: new mission selected as the 7th ESA Earth Explorer Mission."*. EARSel Symposium, Matera, Italy, 2013.

[5] M. Rosengren. "*Improved Technique for Passive Eccentricity Control"*. American Astronautical Society Publication, AAS-89-155, 1989.